Investigation on the sea-state performance of a horizontal axis tidal turbine designed for less energetic flows

Job I. Encarnacion and Cameron Johnstone

Abstract— **Tidal stream turbines are mainly designed to operate in regions with energetic currents that reach velocities greater than 2m/s. The number of sites with this resource is few, making the technology very site-specific relative to other renewable energy devices. Tidal velocities of less than 2m/s would produce less energy but also provides the opportunity for cost reduction due lower expected loads. This potential reduction in cost can be realised in ways other than just downsizing and using cheaper materials. This work analyses the performance of a low-solidity high-TSR rotor aimed to operate at less energetic flows of $U_{tidal} < 2\text{m/s}$. Two cases are evaluated using a quasi-unsteady BEM model implemented in Python 3. The first case evaluates the performance of the rotor when subjected to a sheared (profiled) flow that causes fatigue-inducing, time-varying loads. The second case evaluates the effects of wave-current interaction on the rotor performance. The analysis is done to establish the feasibility of the blade design relative to current industry practice of utilising low-TSR blades that are not subject to cavitation and engineered to withstand far greater loads under high-speed flow ($U_{tidal} > 2\text{m/s}$).**

Keywords— **BEM, Horizontal Axis Tidal Turbine, Low solidity, Low Velocity, Sea-state, TSR**

I. Introduction

THE understanding and development of tidal in-stream devices have been steady in the recent years. However, the utilisation of these devices remains to be highly site-specific as its high cost [1] require the technology to be utilised at high tidal velocities of greater than 2m/s. Extending the technology's suitability to less energetic flows will improve the overall viability of tidal in-stream devices.

South East Asia is dominated by these less energetic flows of $U_{tidal} < 2\text{m/s}$ [2][3], as well as the west coast of the UK [4][5], with majority of the world's oceans falling under this category. This type of flow would generate far less energy; only a quarter of the power extracted in energetic sites may be produced if traditional TSTs are to operate in these regions. Nonetheless, lower structural loading will be experienced, which could translate to lower cost of manufacturing, operation, and maintenance.

The potential reduction in system capital cost may be realised in ways other than just downsizing and using cheaper materials. Current TST design is based on the operation within a typical TSR range (TSR < 4) with a focus on large torque production. This level of torque cannot be attained in lesser energetic flows without severely impacting the device's rotational speed and power production. This reduced torque may be offset by increasing the rotational speed of a rotor, resulting in smaller generators operating at higher rpm for the same amount of power. However, operation of TSTs within a higher TSR range (TSR > 6) is not normally adopted for energetic flows due to the risk of cavitation, although operating at these TSRs may not be a problem in less energetic flows.

A modified NACA 638xx blade with low solidity [6] was found to have a slight reduction in maximum Cp of less than 5% compared to the base NACA 638xx blade [7], with the location of the maximum Cp increasing from TSR ≈ 5.5 to TSR ≈ 6.75. A static simulation found that the stresses on the blade are substantially low.

The performance of the low-solidity high-TSR blade is evaluated and compared to lower TSR blades that are traditionally designed for energetic flows. This work extends the exploration of this low-solidity blade to an unsteady sea-state condition which causes fatigue-inducing, time-varying loads.

II. Numerical Setup

This section serves as summary of the theories used [8] in evaluating the performance of the blades under less energetic flow. Clarifications on inflow mapping are also presented. Implementation of these theories give a quasi-unsteady model which assumes an equilibrium state between the inflow and wake regions of the rotor at every time step.

A. Blade Element Momentum Theory

Much of the working principle behind tidal turbines are built upon the knowledge developed from the wind turbine industry combined with the concepts used for the

Tidal Device Development and Testing #1420

The author is funded to undertake this research by the Philippine Department of Science and Technology (DOST) – Engineering Research and Development for Technology (ERDT).

J.I. Encarnacion is a PhD Researcher in the University of Strathclyde under the supervision of C.M. Johnstone.

design of marine propellers. Blade Element Momentum (BEM) is one of these design and analysis methods used to analyse the performance of the low-solidity NACA blade.

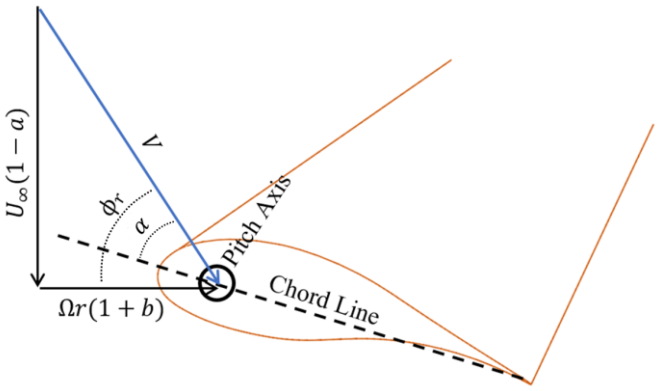

Fig. 1. Velocity triangle for each blade section

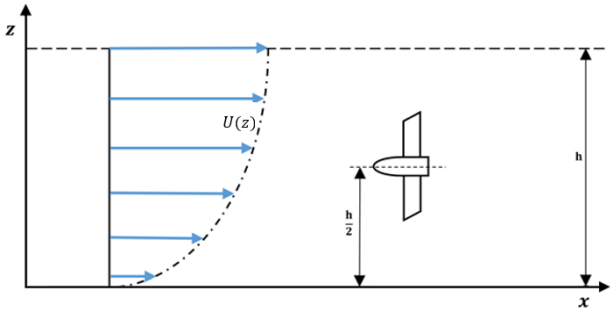

Fig. 2. Power Law Profiled flow for tidal energy sites, $U(z) = U_o z^{1/b}$

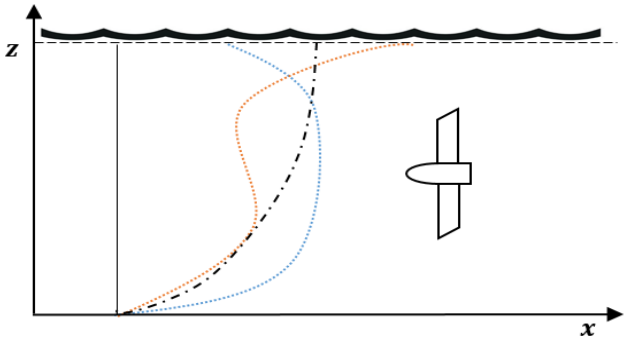

Fig. 3. Sample deformed current profiles under wave action: wave propagating with current (blue) and wave propagating against the current (orange). Lines presented are exaggerated and approximate expected shapes.

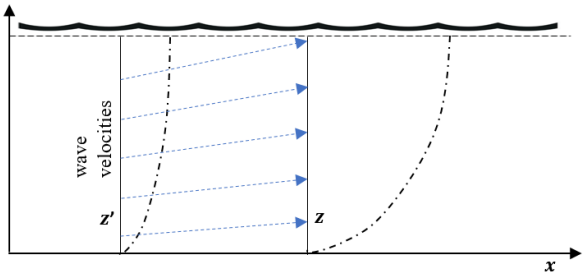

Fig.4. Inflow mapping of z' to z as the axis is stretched due to ocean surface displacement from wave action

BEM integrates the working principle of the blade element (annular stream tube) and the momentum (actuator disc) theories [8,9]. Each theory has two sets of equations that give the thrust and torque of a rotor depending on the values of the axial induction factor, a, and the tangential induction factor, b.

$$\mathrm{dF}_{\mathrm{thrust,\ el}} = B\frac{1}{2}\rho V^2 c_r (C_L cos\phi_r + C_D sin\phi_r)dr$$
$$\mathrm{dF}_{\mathrm{torque,\ el}} = B\frac{1}{2}\rho V^2 c_r r (C_L sin\phi_r - C_D cos\phi_r)dr$$

$$\mathrm{dF}_{\mathrm{thrust,\ disc}} = 4\pi\rho(U_\infty^2 a(1-a) + (b\Omega_r r)^2)rdr$$
$$\mathrm{dF}_{\mathrm{torque,\ disc}} = 4\pi\rho b(1-a)U_\infty \Omega_r^2 dr$$

where the subscripts of $\mathrm{dF}_{\mathrm{thrust}}$ and $\mathrm{dF}_{\mathrm{torque}}$ indicate the theory used (blade element or actuator disc), B is the number of blades, C_L and C_D, are the lift and drag coefficients of the blade element at a flow angle ϕ_r, c_r and Ω_r is the chord and the local tip speed ratio at radius r. V is the total flow when the inflow velocity, U_∞, is combined with the tangential velocity of the blade element as the blade travels along the rotor plane (Figure 1).

$$V = \sqrt{\left(U_\infty(1-a)\right)^2 + \left(\Omega r(1+b)\right)^2}$$

Minimising the error between the blade element and momentum equations maybe achieved by solving the values of a and b iteratively. This is performed in Python 3 using the SciPy.optimize package (method 'SLSQP').

BEM assumes each blade element to be fully independent of each other and does not consider non-ideal flow emanating from the tip and hub sections. This is remedied by using Prandtl tip and hub loss correction factors [10]. The Buhl high induction factor correction corrects for inaccuracies in thrust loads when the axial induction factor exceeds the theoretical limit of about $a >$ 0.4 [11]. Lastly, fixed-pitched rotors such as the ones analysed in this study are subject to the full range of flow and boundary layer regimes including stall conditions. A post-stall model [12] is used to handle these regimes as usage of C_L and C_D values may result in inaccurate results.

B. *Wave-Current Interactions*

The previous equations all assume uniform inflow across the rotor plane. However, tidal sites are subject to a profiled flow (Figure 2) which results in fatigue-inducing time-varying loads. This profile is taken as function of depth, $U(z)$, that may be estimated using a power law:

$$U(z) = U_o\, z^{1/b}$$

where b is usually taken as 7, resulting in a 1/7$^{\mathrm{th}}$ power law in more theoretical simulations.

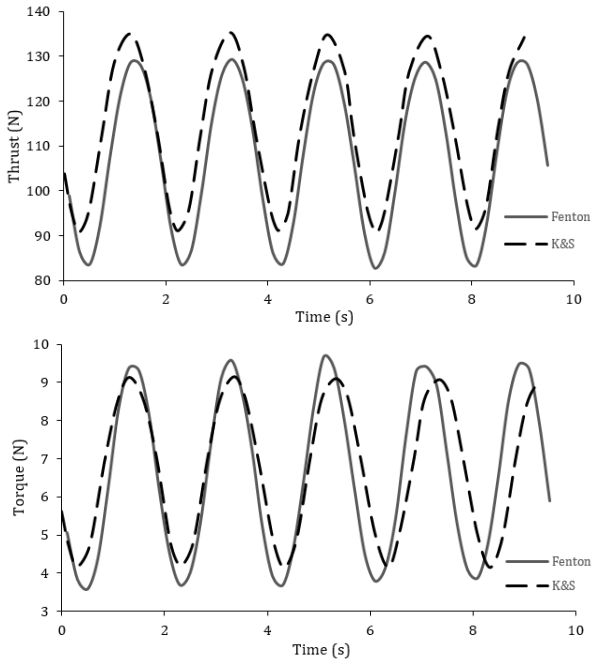

Fig. 5. Rotor torque and thrust loads for quasi-unsteady BEM using coefficients of a) Fenton, and b) Kishida and Sobey: Gaurier W&C1 ($U = 0.67\text{m/s}, \tau = 2\text{s}, H = 0.16\text{m}$)

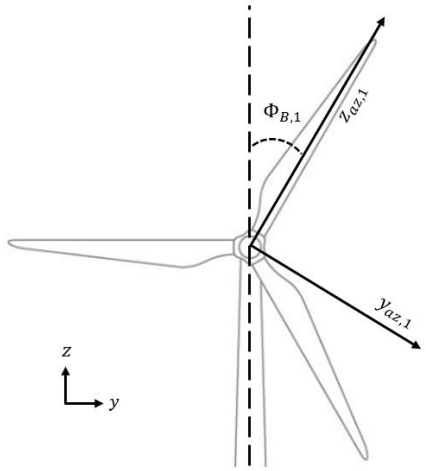

Fig. 6. Representation of transformed azimuthal axes from global axes, x-axis into the page

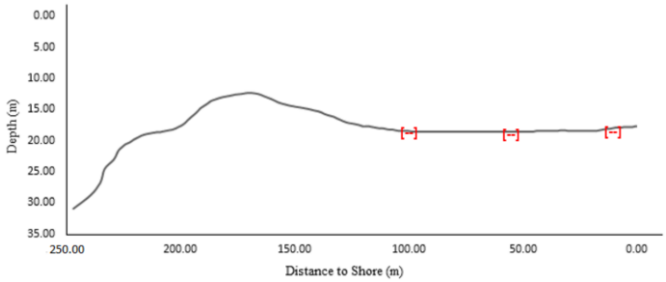

Fig. 7. Location of 10 m windows in a section between Playa del Carmen and Cozumel, distance to shore measured from Cozumel

U_o in this equation is taken as the tidal velocity at the surface. This value is not readily available, hence other forms of $U(z)$ may be used. Utilisation of ADCP measurements allow for the aforementioned form since the power-law function may be fit to the data and obtain a representative flow profile along the water column.

Studies [13]-[16] have shown that waves alter the velocity profile (Figure 3). This effect is included in the BEM simulations by using a three-step kinematic model [17]. The model transforms the inflow, U_∞, to include both wave and tidal velocity components:

$$U(x,z,t) = U_{wave}(x,z',t) + U_{tidal}(x,z)$$
$$W(x,z) = W_{wave}(x,z',t)$$

where U and W are the horizontal and vertical components of wave and tidal velocities. The inclusion of $W_{wave}(x,z)$ alters the previous equation for V to:

$$V = \sqrt{\left(U_\infty(1-a)\right)^2 + \left(\Omega r(1+b) - W_{wave}(x,z',t)\right)^2}$$

U_{wave} is a function of time, t, x and z' as opposed to U_{tidal} being a function of only x and z. The coordinate axes z and z' are both in the vertical direction but vary in values. Waves cause a vertical displacement of the mean water level. Thus, the z axis is stretched, or compressed, to the z' axis to account for this displacement (Figure 4). The values along z' axis are then matched to the values along z using:

$$z' = z + \eta \frac{\sinh(2\pi(z+h)/L)}{\sinh(2\pi h/L)}$$

The three-step kinematic model only provides a method to combine wave and tidal velocity components; it does not solve for the wave velocities independently. Wave velocities are then calculated using existing wave theories. Stokes Theory on waves are applied to the model using the Fenton's approximation [18]. These approximations are based on a uniform inflow current and have been shown to be less accurate [19] compared to the approximations of Kishida and Sobey [20] where wave velocities are solved under a profiled flow. This is due to the presence of vorticity along the water column in a profiled flow. However, comparison of turbine loads under profiled flow using Fenton's approximations and those using Kishida's approximations [21] have shown to be minimal (Figure 5). Fenton's approximations are then adopted due to its relatively simpler approach as implemented in Raschii Python [22].

C. *Time-Varying Velocities*

Velocity at each blade element can easily be calculated using the global axis (Figure 2) but dF_{torque} is not always in the direction of z. Hence, at each time step, the velocities obtained from the three-step kinematic model

are transformed using an azimuthal coordinate system as implemented by Nevalainen [8]. The transformation matrix is as follows:

$$\begin{bmatrix} \dot{x}_{az,\ i} \\ \dot{y}_{az,\ i} \\ \dot{z}_{az,\ i} \end{bmatrix} = \begin{bmatrix} \dot{x}_i \\ \dot{y}_i \\ \dot{z}_i \end{bmatrix} \begin{bmatrix} 1 & 0 & 0 \\ 0 & \cos\Phi_{\mathrm{B},\ i} & -\sin\Phi_{\mathrm{B},\ i} \\ 0 & \sin\Phi_{\mathrm{B},\ i} & cos\Phi_{\mathrm{B},\ i} \end{bmatrix}$$

where Φ_B is the blade angle of the i^{th} blade ($\Phi_{B,1} = 0$) at $t = 0$. This allows for the calculation of the thrust and torque directly as shown in Figure 6.

III. Simulation Cases

D. Blade Geometries

Three blade geometries are used in the simulations:

a) NREL: Low-TSR NREL S814 [23],
b) NACAa: Base Case NACA 638xx [7], and
c) NACAb: Low-Solidity High-TSR NACA 638xx [6].

Using three blade geometries allows for comparison of required torque and resulting loads of a low TSR blade and high TSR blade. In addition, further validation of the design methodology to achieve higher TSRs is done by comparing b) and c). Each blade geometry is also simulated at varying diameters of 4 and 8 meters. Each simulation uses the TSR where maximum C_P is observed for the corresponding blade: $TSR_a = 3.5$, $TSR_b = 5.5$, $TSR_c = 6.75$.

E. Less Energetic Sites

One site from Mexico and another from the Philippines were used as case studies for the simulations. These provide a representative case for sites that are dominated with less energetic flows at $U_{tidal} < 1.5\text{m/s}$.

Mexico

The Cozumel channel has been identified as a specific site where marine energy may be utilised. The flow in the channel is characterised by a constant oceanic current – the Yucatan current. Cozumel island is a protected area, but certain areas may be used for the development of marine energy although only preliminary assessment studies have been performed. ADCP measurements providing snapshots of the flow within the channel were obtained. The characteristic velocity profile, $U(z)$, in a transect is obtained using the averaged values of U_o and b for three 10 m windows (Figure 7).

$$U(z) = 1.136\, z^{1/2.991}, \qquad h_{\text{ave}} = 18.15\text{m}$$

The value of $b = 2.991$ indicates a rougher seabed compared to the bed roughness indicated by the 1/7th power law. Velocities decay faster to 0m/s towards the bottom resulting in higher velocity variation across the rotor. This case provides a quantification of the performance of the low-solidity blade under sheared flow relative to the performance of lower TSR blades.

Philippines

Time-varying ADCP measurements, wave height, and wave period, were obtained for one site in the Philippines. Representative velocity profiles were obtained by using spring and neap tide currents, but it was observed that velocities during neap tides are way too low. Ibañez [24] has shown that there exist greater velocities, but still considered low velocity, for other tidal energy sites. However, since only depth-averaged data are present for other sites, the analysis was still done on the Philippine site where ADCP measurements are available. However, only the characteristic velocity profile, $U(z)$, during neap tide was obtained:

$$U(z) = 0.64\, z^{1/3.500}, \qquad h = 20\text{m}$$

The value of U_o is lower compared to the one obtained for the Mexico case indicating even less extractable energy. The value of b is slightly higher indicating slower decay to 0m/s towards the bottom but should still induce higher load variation across the rotor plane compared to the usual 1/7th power law. In addition to this, increased load variation is introduced by the wave-current interaction. It was found that the significant wave height, $H = 0.5$, propagates with a period of $\tau = 7.3s$. This is considered to be an intermediate depth second-order stokes wave for $h = 20\text{m}$.

This case provides a comparative analysis on the performance under wave-current conditions of the low-solidity blade compared to lower TSR blades.

IV. Results

F. Uniform and Profiled Flow

Rotor Performance

The low-TSR NREL blade produced the lowest power output in both steady and profiled flow. However, this is probably due to the blade geometry generally having a lower peak $C_{P,\max} < 0.4$ compared to the NACA 638xx series blades $C_{P,\max} > 0.4$.

TABLE 1
SIMULATED TORQUE, POWER, AND THRUST FOR 4M ROTORS UNDER STEADY AND PROFILED FLOW CONDITIONS

	F_{torque} (kN)		Power (kW)		F_{thrust} (kN)	
	Steady	Profile	Steady	Profile	Steady	Profile
NREL	1.79	0.61	3.55	1.21	5.89	4.01
NACAa	1.30	0.63	4.06	1.96	5.81	4.09
NACAb	1.03	0.49	3.94	1.89	5.52	3.87

Forces and power drop when going from a steady to a profiled flow mainly because of the drop in the average flow velocities over the whole rotor. The NREL S814 experienced the greatest reduction in loads under profiled with a 65.91% reduction in torque and 31.93%

reduction in thrust loads. This is also attributed to the geometry more than the changing of the TSR location of the maximum C_p as the NACA blades experienced almost the same amount of reduction in loads at ≈52% reduction in torque and ≈30% reduction in thrust loads under a profiled flow.

The low-solidity NACA blade ($TSR_{C_{p,max}} \approx 6.75$) produced 2.88% less power than the base NACA blade ($TSR_{C_{p,max}} \approx 5.5$) under steady flow conditions and 3.60% less power under profiled flow. This is accompanied by a reduction of 20.86% and 21.45% in torque under each respective flow conditions. The large reduction in torque for a very minimal reduction in power output provides a possible cutting of costs in both structural and power transmission components. Similarly, utilisation of the low-solidity NACA blade is favoured over using the low-TSR NREL blade as even higher torque requirements, for the NREL rotor, needs to be applied should the two rotors be designed to have matching power output.

Individual Blade Loads

Load variations under profiled flow are greatest for the NREL blade with 13.65% and 50.81% more variation in thrust and torque than the low-solidity NACA blade. Comparing the base NACA blade to the low-solidity NACA blade isolates the effects of a high-TSR low-solidity design. Thrust and torque variation of the low-solidity NACA blade is 6.32% and 20.19% less than the variation for the base NACA blade.

However, this decrease in load variation is also accompanied by an increase in loading cycles with the NREL blade having only three (3) loading cycles compared to the base NACA blade's five (5) and the low-solidity NACA blade's six (6). This is a major consideration for fatigue studies as the operational TSR of 6.75, relative to the NREL's 3.75, results in twice the loads cycles, potentially halving the life of the blade if loads are not low enough.

Figure 8 shows the load variation for one blade. The same load variation is observed for all other blades offset by each blade's angular spacing.

Effect of Turbine Sizing

TABLE 2
SIMULATED TORQUE, POWER, AND THRUST FOR 8M ROTORS UNDER STEADY AND PROFILED FLOW CONDITIONS

	F_{torque} (kN)		Power (kW)		F_{thrust} (kN)	
	Steady	Profile	Steady	Profile	Steady	Profile
NREL	14.25	4.89	14.16	4.86	23.59	15.95
NACAa	10.43	5.02	16.30	7.83	23.34	16.28
NACAb	82.46	3.94	15.81	7.55	22.13	15.40

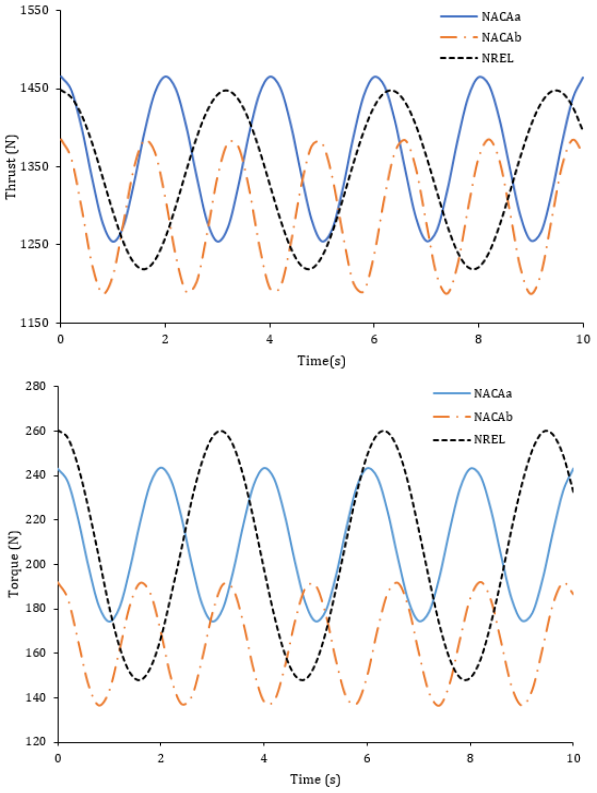

Fig. 8. Torque and Thrust Loads for Blade 1 for 4m diameter turbine case

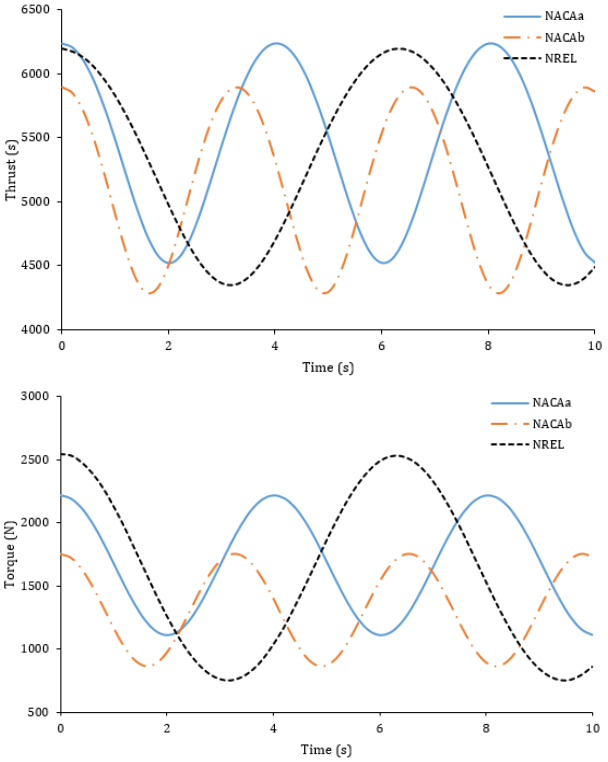

Fig. 9. Torque and Thrust Loads for Blade 1 for 8m diameter turbine case

The same overall trend is observed for 8m diameter rotors. Almost the same relative differences are also obtained (4m vs 8m) with only a slight increase (>0.1%) in the proportion of loads experienced under profiled flow to the loads experienced under steady flow. This may be a function of the highly sheared velocity profile, which results in a more linear relationship when going from small diameter rotors to higher diameter rotors i.e. the average velocity over the whole rotor plane remains roughly the same.

Trends in load variation for individual blade loads are also almost similar with a very slight decrease (>1%) variation for all three geometries. Figure 9 shows the load variation for the 8m diameter turbine. It can be seen that the low-solidity NACA blade still experiences the lowest loads among the three blade geometries.

It can also be observed that the 4m diameter turbine go through more load cycles during 10s of operation compared to the 8m diameter turbine. This is due to higher ω achieved at smaller diameters even with the same TSR.

G. Wave Induced Effects

Rotor Performance

Similar to the previous observations, the NREL produced the lowest power output among the three blades analysed. An initially high-power output from the NREL can be observed although this is mainly due to the computational inaccuracy during the first few seconds of simulation and vanishes towards later time steps (Figure 10).

TABLE 3
SIMULATED POWER FOR WAVE CASES AND COMPARISON WITH PROFILE ONLY CASES FOR 4M DIAMETER TURBINE CASE

	P_{max} (kW)	$\frac{P_{profile}}{P_{wave}}$ max	P_{min} (kW)	$\frac{P_{profile}}{P_{wave}}$ min
NREL	1.43	0.33	0.10	4.56
NACAa	1.34	0.52	0.26	2.64
NACAb	1.30	0.52	0.24	2.78

The peak power output of the NREL matches the peak power output of the low-solidity NACA blade. Nonetheless, the average power output of the low-solidity NACA is 31.95% greater than the NREL across the 10s of simulated operation. This large difference results from the low power output of ≈100W for the NREL and ≈250W for the low-solidity NACA blade. The median value of the relative difference between two blades provides a time-based quantification of how much the other blade outperformed the other. This was obtained to be at 12.19% indicating that the low-solidity NACA blade produces at least 12.19% more power half of the time both operated.

The difference in power output for the base NACA blade and the low-solidity NACA blade remains to be small with the base NACA blade producing 4.23% more power on average. Table 3 summarises the power outputs of the blades and it was observed that the base NACA always produced greater power than the NREL blade. This is a function of $C_{P,max}$ as discussed previously.

Higher deviation from the profiled power output is observed for the NREL blade as it goes from a maximum of 33% of the profiled flow power output to more than a quarter at minimum power output under the wave case. This indicates that the NREL blade is more sensitive to wave action for the given wave parameters.

Isolating the effects of going into higher TSR, it appears that the maximum power output attained by the lower solidity NACA blade has a similar proportion to the maximum power output of the base NACA blade. However, the minimum power output of the latter still remains to be nearer to its profiled power output indicating that the lower solidity blade is slightly more sensitive to wave action for the given wave parameters.

Individual Blade Loads

Individual thrust loads for the NREL is always higher than low-solidity NACA. The three NREL blades are under 5.15% more thrust load, and at least 5.08% more thrust load half of the time that both are in operation. A larger difference is seen for torque loads as the NREL blades are subject to an average 41.87% more torque, and at least 44.31% more torque half of the time.

This decreased torque in the low-solidity NACA blade results in lower overall loads which allows for the utilisation of smaller generators in the turbine design. In addition to construction costs, reduced installation costs are possible due to reduced weight.

Effect of Turbine Sizing

Increasing the turbine diameter does not change the observed trends for rotor performance although there is a greater relative difference between the performance of the NREL blade compared to low-solidity NACA blade with the latter producing 33.41% more power, about 1.5% more than the previous 4m diameter turbine. There is also an increase in the median relative difference between the low-solidity NACA producing 11.5% more power, compared to the 10.29% in the 4m diameter case, and the NREL half of the time turbines are operational.

TABLE 4
SIMULATED POWER FOR WAVE CASES AND COMPARISON WITH PROFILE ONLY CASES FOR 8M DIAMETER TURBINE CASE

	P_{max} (kW)	$\frac{P_{profile}}{P_{wave}}$ max	P_{min} (kW)	$\frac{P_{profile}}{P_{wave}}$ min
NREL	5.27	0.35	0.39	4.75
NACAa	5.38	0.52	1.03	2.69
NACAb	5.21	0.51	0.95	2.84

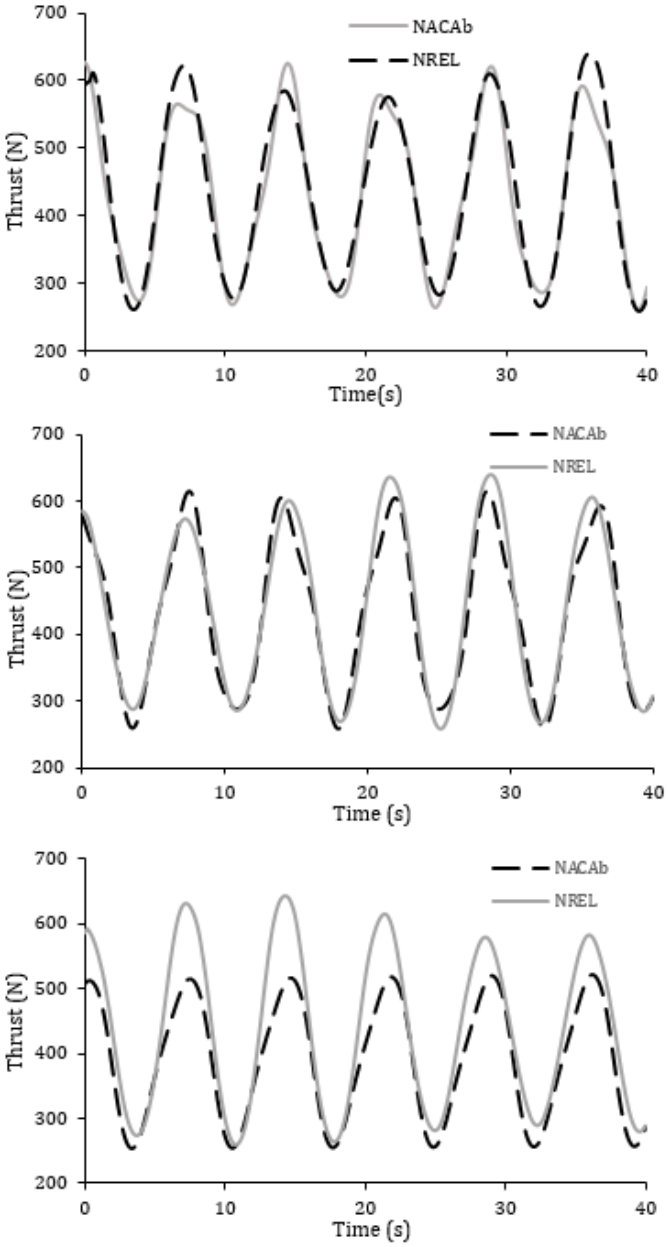

Fig. 10. Individual Thrust Loads for Blade 1, 2, and 3 (top to bottom) for 4m diameter turbine case

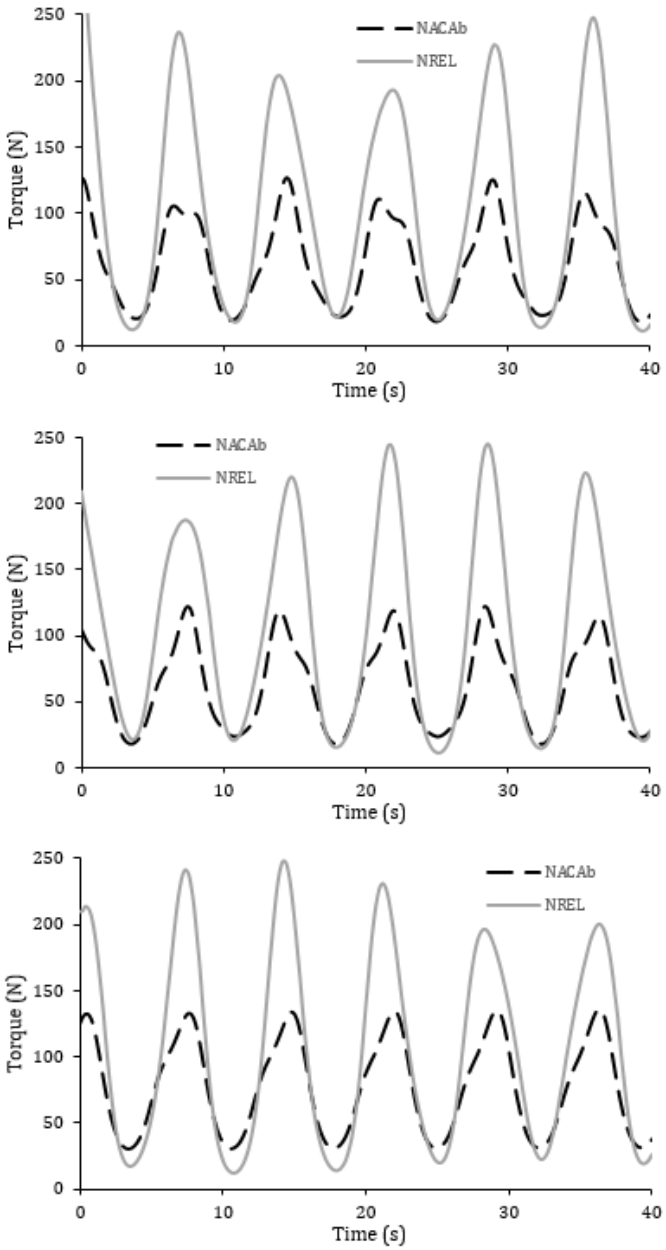

Fig. 11. Individual Torque Loads for Blade 1, 2, and 3 (top to bottom) for 4m diameter turbine case

The same trends in terms of sensitivity to wave action is observed for the 8m diameter cases although there is a slight increase in the proportions at minimum power output. This is due to the increased exposure of the rotor to wave velocities near the surface wherein velocities at minimum power output reduce the flow over the blades. There is also a notable difference between the difference in minimum power outputs of the NREL blade to the two NACA blades as the diameter is increased. The 4m diameter NREL produced only half of the NACA power outputs at minimum production. However, the 8m diameter NREL sees an even bigger difference with the rotor only generating 40% of the power outputs of the NACA at minimum production.

The difference between individual thrust loads decrease to just about an average of 1.97% compared to the former 5.15%. This is, however, accompanied by an increase in the difference for individual torque loads with the NREL being under 55.83% more torque load compared to the former 44.31% in the 4m turbine case. This apparent difference in trends for torque and thrust indicate two possible cost reduction strategies.

a) The decreasing difference of thrust loads as turbine diameter increases encourages the use of smaller diameter turbines as more savings from structural costs may be realised.
b) The increasing difference of torque loads encourages the use of larger diameter turbines as more savings from generator sizing may be realised when comparing the NREL and low-solidity NACA.

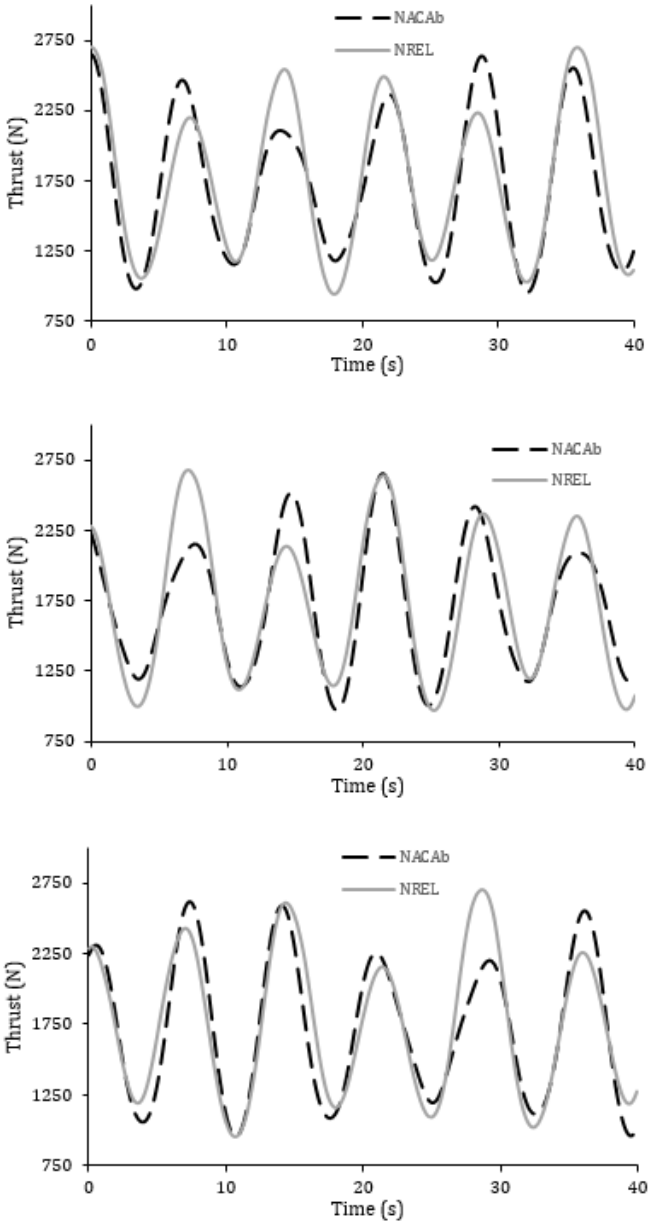

Fig. 12. Individual Thrust Loads for Blade 1, 2, and 3 (top to bottom) for 8m diameter turbine case

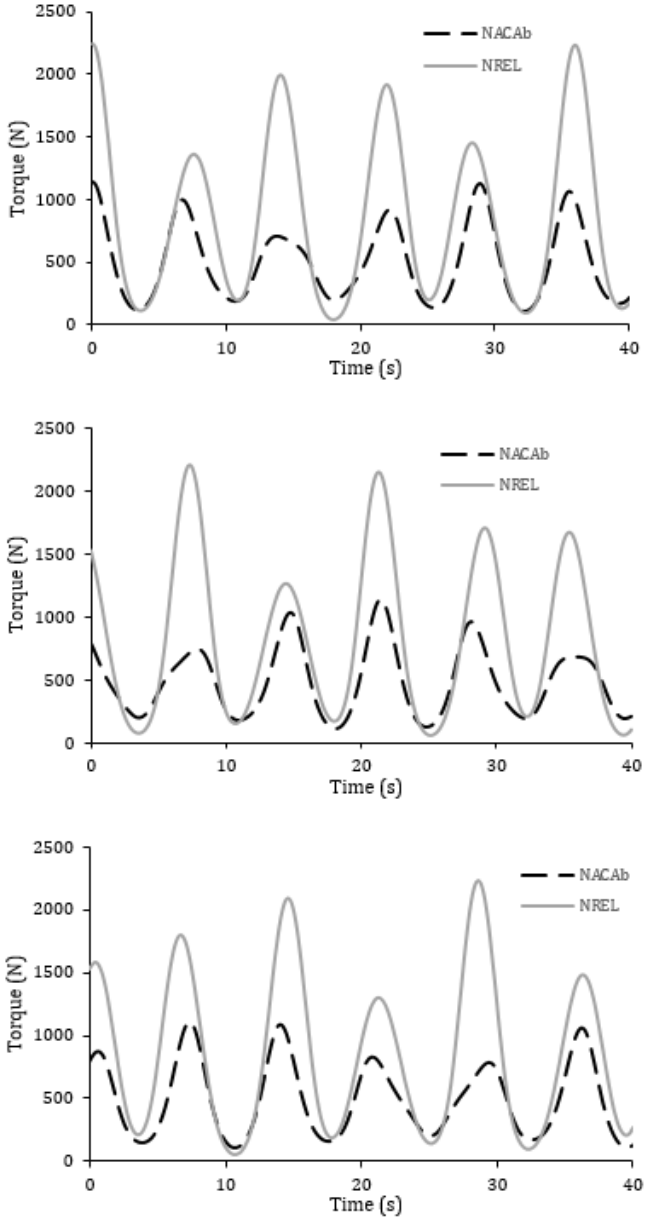

Fig. 13. Individual Torque Loads for Blade 1, 2, and 3 (top to bottom) for 8m diameter turbine case

V. Future Work

Fitted profiles in this work reveal that the 1/7th power law does not necessarily apply to less energetic sites. The resulting values indicate a thicker boundary layer and highly sheared flow compared to the characteristic flow found in energetic sites. Additional data should be used to verify if this characteristic of less energetic sites.

Dynamic response of the blade must be included in the BEM model to account for the changing inflow conditions. A quasi-unsteady approach assumes equilibrium between the inflow and wake of the turbine which hardly ever happens. This can be done by adding in inertial effects and added mass effects as have been implemented in the ESRU MATLAB code.

High-TSR blades pushes the boundaries of operation towards cavitation limits. Current installations are engineered so that cavitation will not be an issue, hence favouring lower TSR blades. The design methodology should be extended to include cavitation studies and possible control strategies to minimise this risk, among others.

Experimental validation with low-solidity NACA blade is also needed as having very slender blades leads to losses due to possible excessive deflection. Deflections may be minimised by the careful material selection.

It is also important to isolate the effects of going into higher TSR. The benefits of designing a blade that has a high as possible TSR designed operation may be verified by taking the NREL S814 blade and further designing it to achieve TSRs similar to the low-solidity NACA. Comparing the performance of such blade would provide information if such a design methodology is viable not only for the NACA blade, but possibly any blade geometry.

ACKNOWLEDGMENT

Part of the data used in this paper was obtained through Newton Fund Institutional Links and CONACYT-SENER-Fondo de Sustentabilidad Energetica-Institutional Links under grants IL5 332324562 and 291380. Additional data was also provided by OceanPixel Ltd.

REFERENCES

[1] S. Astariz, A Vazquez, and G. Iglesias. Evaluation and comparison of the levelized cost of tidal, wave, and offshore wind energy. Journal of Renewable and Sustainable Energy 7(5), 053112, 2015 doi:10.1063/1.4932154

[2] [M.D. Bausas., O.D.G. de Luna and M.R.C.O Ang. Tidal In-stream Energy Resource and Conversion Device Suitability Analysis in the Northern Philippines. Proceedings of Asian Conference on Remote Sensing. 2016.

[3] [M.A.J. Quirapas, H. Lin, M.L.S. Abundo, S. Brahim and D. Santos. Ocean Renewable Energy in South East Asia: A Review. Renewable and Sustainable Energy Reviews 41 pp.799-817. 2015

[4] D. Haverson, J. Bacon, H.C.M. Smith, V. Venugopal and Q. Xiao. Cumulative impact assessment of tidal stream energy extraction in the Irish Sea. Ocean Engineering 137 pp. 417-428, 2017 doi:10.1016/j.oceaneng.2017.04.003

[5] R.C. Roche, K. Walker-Springett, P.E. Robins, J. Jones, G. Veneruso, T.A. Whitton, M. Piano, S.L. Ward, C.E. Duce, J.J. Waggitt, G.R. Walker-Springett, S.P. Neill., M.J. Lewis and J.W. King. Research priorities for assessing potential impacts of emerging marine renewable energy technologies: Insights from developments in Wales (UK). Renewable Energy 99 pp. 1327-1341, 2016 doi:10.1016/j.renene.2016.08.035

[6] J. I. Encarnacion, C.M. Johnstone. Preliminary Design of a Horizontal Axis Tidal Turbine for Low-Speed Tidal Flow. Proceedings of the 4th Asian Wave and Tidal Energy Conference. 2018

[7] Bahaj, A.S., Molland, A.F., Chaplin, J.R., and Batten, W.M.J Power and Thrust measurement of marine current turbines under various hydrodynamic flow conditions in a cavitation tunnel and a towing tank. Renewable Energy 32: 407-426, 2007.

[8] T.M. Nevalainen. The Effect of Unsteady Sea Conditions on Tidal StreamTurbine Loads and Durability. PhD Thesis. University of Strathclyde, 2016

[9] G. Ingram. Wind turbine blade analysis using the blade element momentum method version 1.0. School of Engineering, Durham, UK. 2005

[10] W.Z. Shen, R. Mikkelsen, J.N. Sorensen and C. Bak. Tip loss correction factors for wind turbine computations. Wind Energy 8.4. 2005

[11] J.F. Manwell, J.G. McGowan, and A.L. Rogers. Wind Energy Explained: Theory, Design and Application. 2nd ed, Wiley & Sons, 2009.

[12] D. Spera. Wind Turbine Technology: Fundamental Concepts of Wind Turbine Engineering. American Society of Mechanical Engineers, 1994. turbines

[13] M. Olabarrieta, R. Medina, S. Castanedo. Effects of wave-current interaction on the current profile. Coastal Engineering 57, 643-655, 2010

[14] P.H. Kemp, R.R. Simons. The interaction between waves and a turbulent current: waves propagating with the current. Journal of Fluid Mechanics 116, 1982.

[15] G. Klopman. Vertical structure of the flow due to waves and currents. Progress report H840.30, Part II. Delft Hydraulics. 1994..

[16] M. Umeyama. Reynolds stresses and velocity distributions in a wave–current coexisting environment. Journal of Waterway, Port, Coastal and Ocean Engineering 131 (5), 2005.

[17] R. Dalrymple, J. Heidman. Nonlinear Water Waves on a Vertically Sheared Current. Wave and Current Kinematics and Loadings Report No. 3.12/156, 1989.

[18] J. Fenton. A Fifth-Order Stokes Theory for Steady Waves. Journal of Waterway 111, 1985.

[19] C. Swan. An Experimental Study of Waves on a Strongly Sheared Current Profile. Proceedings of the 23rd International Conference of Coastal Engineering, 1992

[20] N. Kishida, R.J. Sobey. Stokes theory for waves on linear shear current. Journal of Engineering Mechanics, ASCE Vol.114 1317-1334, 1989

[21] T.M. Nevalainen. C.M. Johnstone, A.D. Grant. An Unsteady Blade Element Momentum Theory for Tidal Stream Turbines with Morris Method Sensitivity Analysis. Proceedings of the 11th European Wave and Tidal Energy Conference, 2015

[22] T. Landet. Raschii 1.0.2 [Python]. https://pypi.org/project/raschii/

[23] N. Barltrop, K.S. Varyani, A. Grant, D. Clelland, X.P. Pham. Investigation into wave-current interaction in marine current turbines. Proceedings of IMechE 221 A 223-241, 2007

[24] R. Ibañez, T. Mañalac, N. Chua. Tidal Current Resource Power quantification using NAMRIA data sets of the Philippines. 11th AUN/SEED-Net Regional Conference on Energy Engineering, 2018